Sensors and Actuators B 247 (2017) 540–545

Contents lists available at ScienceDirect

Sensors and Actuators B: Chemical

journal homepage: www.elsevier.com/locate/snb

Hydrogen sulfide gas sensor based on graphene-coated tapered photonic crystal fiber interferometer

Xu Feng[a,b], Wenlin Feng[a,b,*], Chuanyi Tao[a], Dashen Deng[a], Xiang Qin[a], Rong Chen[a]

[a] Department of Physics and Energy, Chongqing University of Technology, Chongqing 400054, China
[b] Chongqing Key Laboratory of Modern Photoelectric Detection Technology and Instrument, Chongqing 400054, China

ARTICLE INFO

Article history:
Received 1 January 2017
Received in revised form 11 March 2017
Accepted 14 March 2017
Available online 18 March 2017

Keywords:
Graphene
Mach-Zehnder interferometer
Photonic crystal fiber
Gas sensor
Hydrogen sulfide

ABSTRACT

A hydrogen sulfide gas sensor based on graphene-coated tapered photonic crystal fiber (GTPCF) Mach-Zehnder interferometer (MZI) was proposed and experimentally demonstrated. The GTPCF-MZI is formed by fusion splicing a short length of tapered PCF between two single-mode fibers. The air holes of PCF in the splicing regions are fully collapsed and so that it is conducive to the mode coupling. The GTPCF-MZI was coated with a layer of graphene by using a dip-coating and sintering process. Experimental results show that with the increasing concentration of hydrogen sulfide, the interference spectra appear blue shift. In addition, a high sensitivity of 0.03143 nm/ppm and a good linear relationship are obtained within a measurement range from 0 to 45 ppm. The sensor has the advantages of simple structure, high sensitivity, easy manufacture and low cost, and can be used in indoor gas sensing fields such as factories and laboratories and so on.

© 2017 Elsevier B.V. All rights reserved.

1. Introduction

Hydrogen sulfide (H_2S), which is well known as a very poisonous, corrosive, flammable, and explosive gas, is produced from the prokaryotic breakdown of organic matter in the absence of oxygen gas, such as in sewers and swamps. It also occurs in volcanic gases, natural gas, and in some sources of well water. The toxicity of hydrogen sulfide is comparable with that of carbon monoxide. 320–530 ppm leads to pulmonary edema with the possibility of death [1]. Thus, those used by utility, sewage and petrochemical workers, are set to alarm at 10 ppm and to go into high alarm at 15 ppm for personal safety.

On one hand, graphene, which has many unusual properties, is an allotrope of carbon in the form of a two-dimensional, atomic-scale, hexagonal lattice in which one atom forms each vertex. Graphene has unique optical properties with an unexpectedly high opacity and huge specific surface area for an atomic monolayer, therefore, it is suitable for gas sensing material [2,3]. The improving gas sensing properties of graphene was investigated by the first-principle calculation [4]. Flexible and transparent gas molecule sensor integrated with sensing and heating graphene layers was proposed by C.G. Choi, and Y.J. Yu, et al. [5]. On the other hand, photonic crystal fibers (PCFs), also called microstructured optical fibers, which hold unique guiding mechanisms and modal properties that are impossible with traditional optical fibers, have a lot of applications in the fiber-based sensors [6–29]. However, to the best of our knowledge, the research reports of the gas sensing sensor combining graphene with photonic crystal fiber is not yet seen. Thus, a Mach-Zehnder interferometer (MZI) gas sensor based on graphene-coated tapered photonic crystal fiber (GTPCF) is presented in this work. This sensor is easy to manufacture and only needs to be spliced with the common single mode fiber (SMF) at the two ends of the tapered photonic crystal fiber (PCF), and then graphene was coated on the surface of PCF. The graphene-coated tapered photonic crystal fiber (GTPCF) can enhance the coupling between core mode and cladding mode. Therefore, the sensitivity of the sensor can be improved effectively. As an application, hydrogen sulfide gas was detected by using the GTPCF interferometer and some useful results were obtained.

2. Experimental

2.1. Principle of operation

The schematic diagram of the GTPCF-MZI is shown in Fig. 1(a). After tapering the PCF, a strong evanescent field is formed near the tapered region and makes the susceptible to the refractive index variations of the external coated membrane. As shown in Fig. 1(a),

* Corresponding author at: Department of Physics and Energy, Chongqing University of Technology, Chongqing, 400054, China.
E-mail addresses: wenlinfeng@126.com, fengwenlin@cqut.edu.cn (W. Feng).

http://dx.doi.org/10.1016/j.snb.2017.03.070
0925-4005/© 2017 Elsevier B.V. All rights reserved.

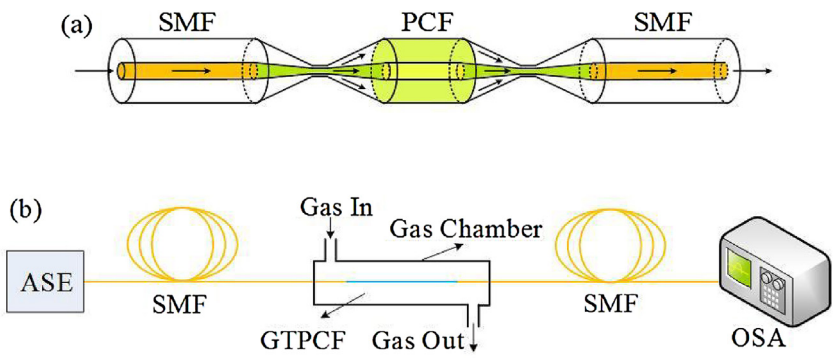

Fig. 1. (a). Schematic diagram of GTPCF-MZI structure; (b). Schematic diagram of the experimental setup.

when light travels from the SMF to the tapered PCF, the core mode of SMF begins to diffract, i.e., after the first splice, a part of the light is coupled to PCF in the transmission of core mode, and another part of light is coupled to the cladding with the transmission of cladding mode. In this process, the propagation constants between the core mode and cladding mode of GTPCF are different. After the transmission distance L, there will be a phase delay between the two modes. Finally, when the two parts of lights arrive at the second splice, the cladding mode of the sensing region and the core mode of the GTPCF will be interfered in the second input port of SMF, that is, Mach-Zehnder interference. Thus, the phase delay of the two modes of interference and the central wavelength of the interference are, respectively, expressed as [30–32]

$$\varphi = \frac{2\pi(n_{eff}^{co} - n_{eff}^{cl})L}{\lambda} = \frac{2\pi\Delta n_{eff}L}{\lambda} \quad (1)$$

$$\lambda_m = \frac{\Delta n_{eff}L}{m} \quad (2)$$

where n_{eff}^{co} and n_{eff}^{cl} are the effective refractive indices of core and cladding modes, respectively. L is the distance between the two coupling points corresponds to the physical length of the interferometer and λ is the wavelength of incident light. $\Delta n_{eff}(=n_{eff}^{co}-n_{eff}^{cl})$ is the difference between the effective refractive indices of core and cladding modes. λ_m is the m^{th}-order wavelength of interference. When the coated-graphene absorbs the target gas, the refractive index of the cladding in tapered PCF's evanescent field changes, and then n_{eff}^{cl} and Δn_{eff} will change together. The m^{th}-order shift $\Delta\lambda_m$ can be given as

$$\Delta\lambda_m = \frac{(\Delta n_{eff} + \Delta n)L}{m} - \frac{\Delta n_{eff}L}{m} = \frac{\Delta nL}{m} \quad (3)$$

in which $\Delta\lambda_m$ is the m^{th}-order wavelength shift of interference. Δn is the difference between the refractive indices of the target gases of different concentrations. From Eq. (3), the shift in the interference fringes is a function of Δn when L is a definite value.

As shown in Fig. 1(b), a broadband amplified spontaneous emission (ASE) source is launched into the structure of GTPCF. When two (core and cladding) modes of light arrive at the second collapsed region, the interfere is formed. Transmission spectra can be monitored by using an optical spectrum analyzer (OSA, Yokogawa, AQ6370D).

2.2. Fabrication of the GTPCF-MZI

For the fabrication of the GTPCF-MZI, the PCF was sandwiched between two SMFs and then tapered via a fiber fusion splicer (Furukawa Electric Co. Ltd., S178C). A 5-cm-long PCF (YOFC, TIR-PCF) and SMF (SMF-28) were employed for a lower fusion loss because they have the same diameter. The cross section of PCF used in the sensing experiment is shown in Fig. 2(a). As depicted in Fig. 2(b), two SMFs, are respectively, spliced two ends of PCF. The air holes of the PCF around the ends were fully collapsed during the fusion splicing. And then, the fusion splicer can accurately control the motor to draw the middle section between SMF and PCF, and forms a taper.

It should be pointed out that the automatic operation mode of the splicer is used for splicing and tapering the standard SMF and PCF. In the operation program of the splicer, the default parameters for the splicing of the SMF and PCF are as follows: the first and second arc-power setting at 100, the initial and second end arc-power setting at 40, the cleaning duration time of 200 ms, the prefusion time of 160 ms, the initial arc-duration time of 1 s, the second arc-duration time of 2 s, the Z-pull time of 1 s, and Z-pull distance of 400 μm. The arc-duration time, arc-power and Z-pull distance can influence the size of the waist and length of transition zone of the taper. Generally, the bigger Z-pull distance can obtain the smaller size of the waist and longer length of transition zone of the taper.

The GTPCF were prepared by a dip-coating and sintering process. Firstly, the isopropanol and the monolayer graphene nanopowders are fully mixed according to the stoichiometric ratio, and then the above prepared tapered PCF is put into the mixed solution for dipping coating. Secondly, put the graphene-coated tapered PCF into the vacuum drying box with drying at 80 °C for 6 h. Lastly, put it into the tubular furnace to sinter at 350 °C for 2 h under the protection of nitrogen, and then the GTPCF was obtained. The graphene-free and graphene-coated tapered PCF are shown in Fig. 2(b) and (c), respectively. Compared Fig. 2(b) with (c), the isopropanol dispersed graphene evenly distributed on the surface of the tapered PCF, and by calcining, has been formed on the surface of a film thickness of about 80 nm (see Fig. 2(d)). It should be noted that the thickness of the graphene film can be controlled by the concentration of graphene solution, dip-coating time, etc. In this experiment, the greater concentration of graphene can get the thicker graphene film.

3. Results and discussion

Based on successful fabrication of GTPCF-MZI, the gas sensing test was performed according to the sensor system of Fig. 1(b). The left and right ends of the gas chamber are respectively sealed by epoxy resin, and the upper and the lower two parts of the gas chamber are respectively the inlet and outlet of the measured gas. All the measurements were carried out at room temperature (about 20 °C).

Different concentrations of hydrogen sulfide can be prepared by mixing the nitrogen gas. Transmission spectra of the GTPCF-MZI before and after coating with graphene were recorded for comparison in Fig. 3. The results indicate that the contrast was slightly reduced but still enough high with an obvious wavelength shift.

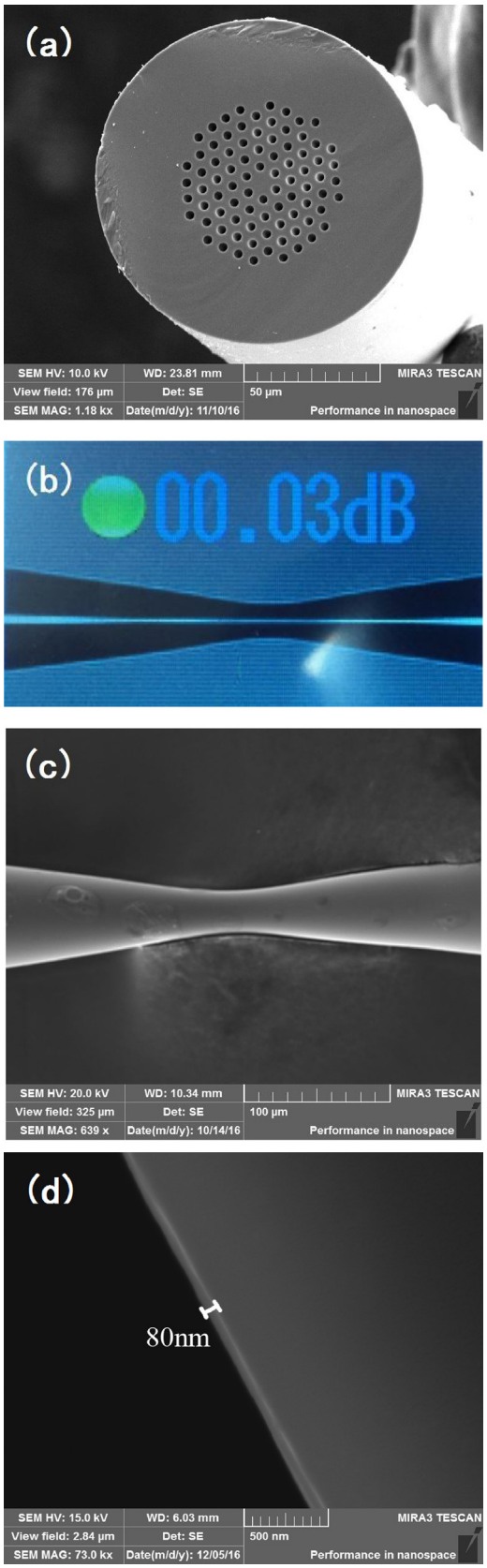

Fig. 2. (a) The cross section of PCF used in the sensing experiment; (b). The structure of tapered PCF before coating; (c). The structure of tapered PCF after coating; (d). The scanning electronic microscope (SEM) image of the cross-section of the tapered fiber coated with graphene film.

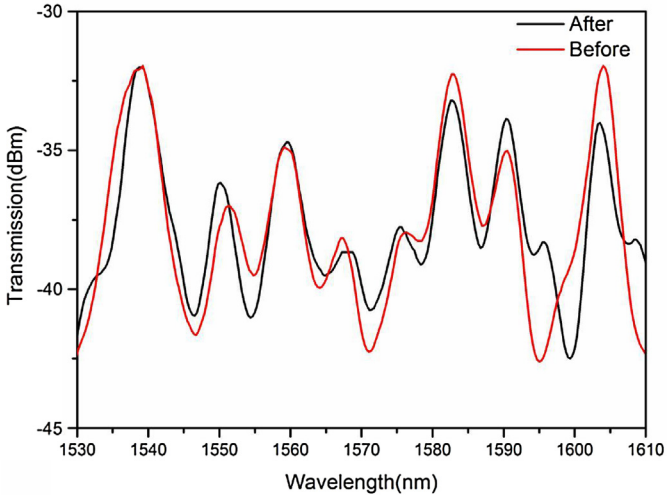

Fig. 3. Transmission spectra of the GTPCF-MZI before and after coating with graphene.

Different concentrations (5 ppm, 10 ppm, 15 ppm, until 45 ppm) of hydrogen sulfide gas were prepared and the spectral responses of GTPCF sensors to different concentrations of hydrogen sulfide were recorded by the OSA (Fig. 4(a)). As shown in Fig. 4(a), there is an obvious interference phenomenon observed by the OSA. Clearly, the transmission dip shifted to shorter wavelength with the increasing of hydrogen sulfide concentration. The reason is as follows: When the hydrogen sulfide gas contacts with the sensing layer of graphene of GTPCF, the effective refractive index of the cladding will be increased, but the refractive index of the core is unchanged, thus, the difference value (Δn_{eff}) of refractive index is decreasing. Therefore, the formula (2) shows that with the increase of hydrogen sulfide gas concentration, the output transmission spectra of the sensor will be blue shifted. The experimental results are in good agreement with the theoretical analysis.

The data of dip wavelength vs. concentration was fit by a linear regression model. The result showed that the correlation coefficient R^2 of the calibration curve was about 0.99636 (Fig. 4(b)), which indicated a fairly good linear response of the GTPCF sensor in the given hydrogen sulfide concentration range. The sensitivity of the graphene to hydrogen sulfide was estimated to be 0.03143 nm/ppm.

The transmission spectra was recorded every 20 s in order to determine the dynamic behavior of the sensor. Fig. 5 shows the dynamic response of GTPCF hydrogen sulfide sensor. As shown in Fig. 5, all the points were the peaks of the transmission spectrum. The interference dips was shifted from 1555.7 nm and 1554.3 nm when GTPCF put into the two hydrogen sulfide alternately, it has showed excellent reversible performance. In addition, the dynamic response time (t_r) and recovery time (t_f) of the GTPCF hydrogen sulfide sensor were about 60 s and 80 s, respectively.

The selectivity of the sensor was tested for hydrogen sulfide and several other gases (Fig. 6). When the sensor was immersed in nitrogen, carbon dioxide, and argon, respectively, no remarkable changes were observed. The sensor exhibited extremely sensitivity toward hydrogen sulfide as compared to other gases, which shows relative wavelength shifts less than 10% of that measured in response to exposure to the hydrogen sulfide gas at 45 ppm. The current sensor shows a better selectivity to hydrogen sulfide compared with other gases which indicates that it can be combined with the film better.

As is known to all, graphene is a kind of sensitive material with huger surface area than that of other's nanomaterials. On one hand, when the gas molecules adsorbed on the surface of graphene, the

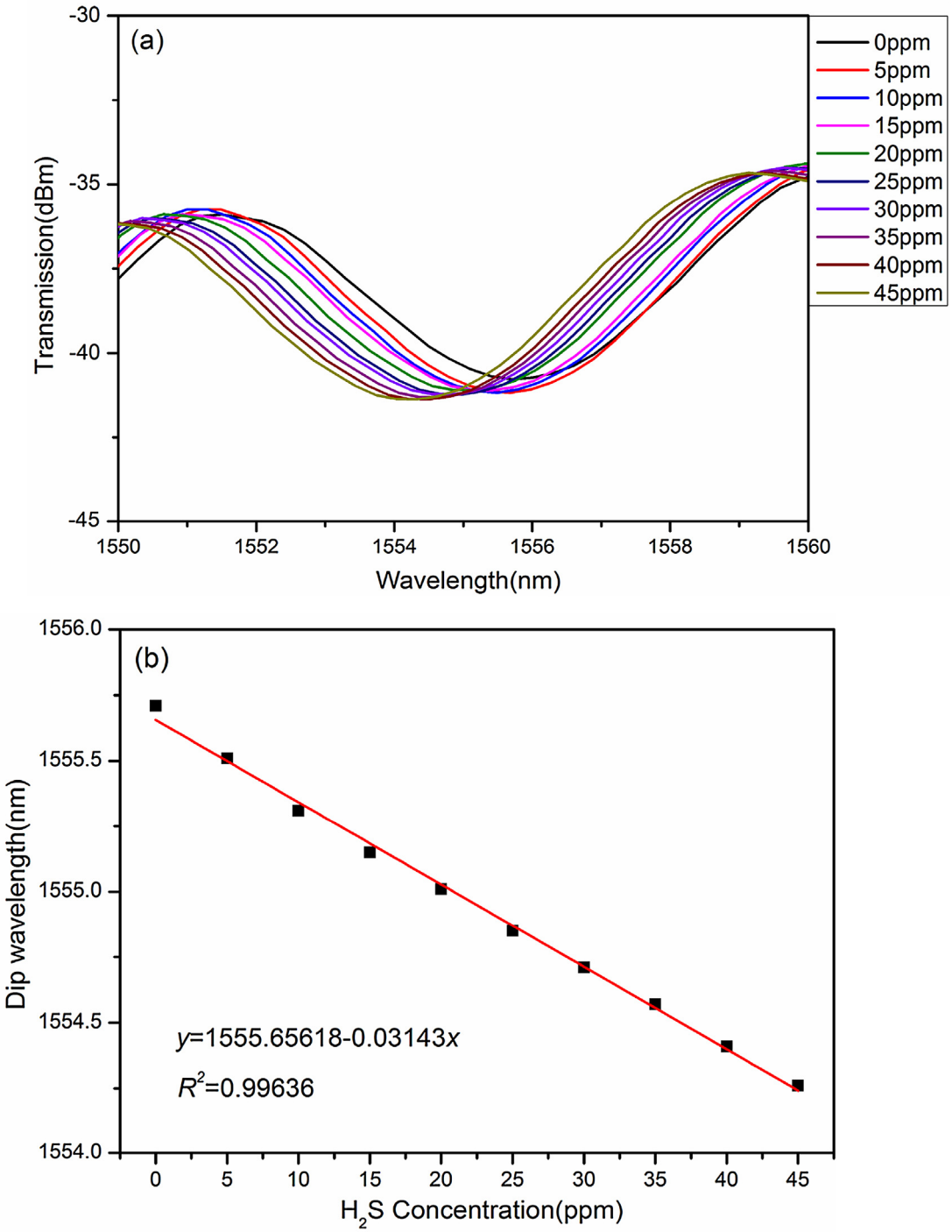

Fig. 4. (a). The spectral responses of the GTPCF sensor in various concentrations of hydrogen sulfide; (b). The wavelength shift upon the concentration of hydrogen sulfide.

carbon atoms of graphene will push each other and the lattice constant will be also changed by the Van der Waals force, which will influence the spatial distribution of carriers, and induce the change of the local dielectric constant of graphene. On the other hand, each carbon atom of graphene has a lone electron, and the electronic activity is very strong due to its special hexagonal structure and π bond. Thus, the gas molecules, as donors or acceptors, absorb easily on the surface of graphene, and form the electron- or hole-doped graphene. Therefore, the conductivity and dielectric constant of graphene will be changed, and then the optical refractive index of graphene film of the cladding area will be also varied with the change of the spatial distribution of carriers, conductivity and dielectric constant. In this study, hydrogen sulfide is polar molecule, but the nitrogen, argon and carbon dioxide are non-polar, therefore the graphene nanocoating photonic crystal fiber sensor for hydrogen sulfide showed better gas sensing and selectivity properties than the other three gases. What's more, the proper length of PCF can be obtained by the optimal interference experiment. After the adsorption of the target gas, the too long length of PCF may induce worse interference because the cladding mode decays quickly, and the too thickness of graphene film may cause the change of refractive index or the interference is not obvious. Therefore, the 80 nm thickness of graphene film is adopted and the interference is obvious in this experiment. Considering the smaller

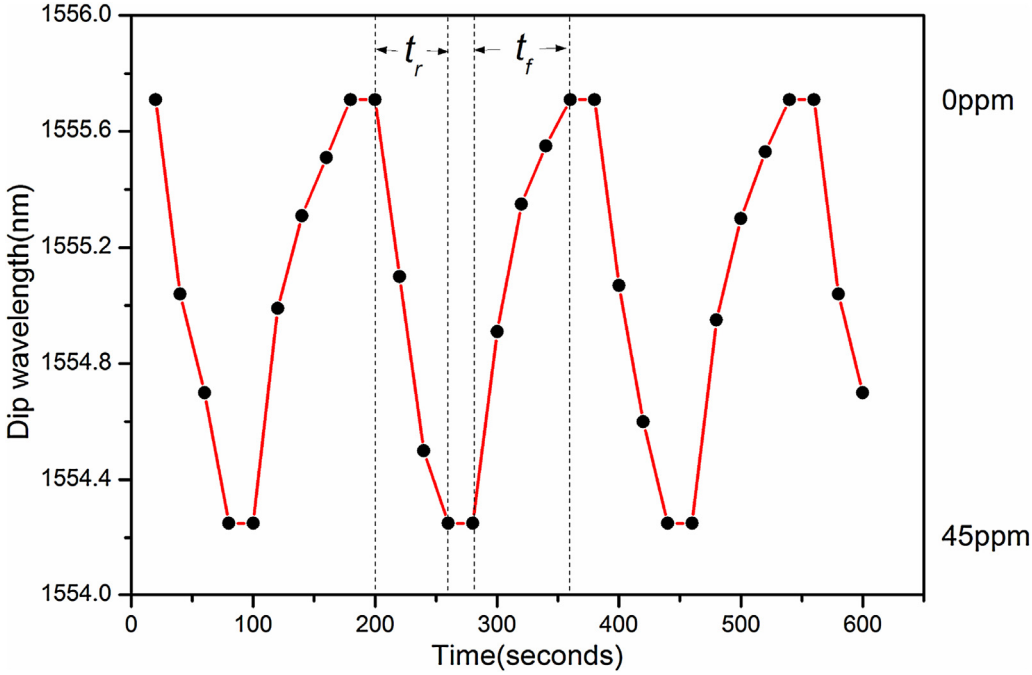

Fig. 5. Dynamic responses of the GTPCF hydrogen sulfide sensor.

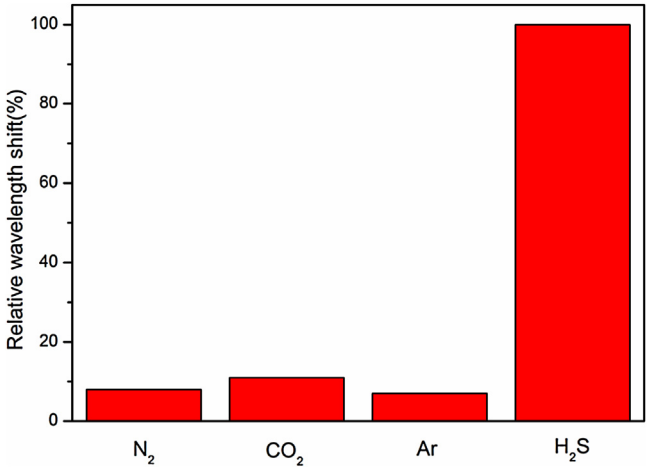

Fig. 6. Relative wavelength shifts of the transmission spectrum of the GTPCF for hydrogen sulfide, nitrogen, carbon dioxide and argon.

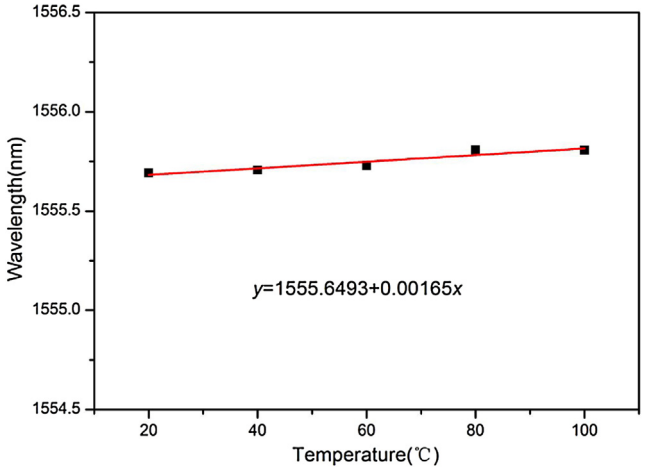

Fig. 7. Relationship between wavelength and temperature.

size of the waist is more fragile, and longer length of transition zone of the taper may not be economically applicable, thus, in this experiment, the 40 μm size of the waist and the length 400 μm of transition zone of the taper are used for a taper.

In order to illustrate the practical application and a better understanding for the proposed sensor characteristics, the temperature cross sensitivity is investigated. As shown in Fig. 7, the temperature sensitivity is 0.00165 nm/°C in the range of 20–100 °C for the measurement of hydrogen sulfide. It shows that the sensor is insensitive to the temperature and can overcome the temperature cross sensitivity. This result is consistent with that of some literatures [32–34].

4. Conclusions

In summary, a method of fast response fiber-optic hydrogen sulfide sensor is demonstrated based on the graphene-coated tapered photonic crystal fiber Mach-Zehnder interferometer. The results showed that with the increase of hydrogen sulfide concentration, the dip wavelength of the transmission spectrum presents blue shift, and the sensitivity is 0.03143 nm/ppm in the range of 0–45 ppm of the concentration of hydrogen sulfide. It displays a good linear response, high sensitivity and selectivity to hydrogen sulfide. The response time of GTPCF sensor is 60 s. This work provides a general approach for fabricating graphene film for fast response GTPCF hydrogen sulfide sensor, and it is also could be candidate for environmental monitoring, toxic workplaces, and chemical analysis.

Acknowledgments

This work was supported by the National Natural Science Foundation of China (Grant nos. 51574054 and 51304260), the University Innovation Team Building Program of Chongqing (Grant no. CXTDX201601030), and the Postgraduate Research Innovation Project of Chongqing (Grant nos. CYS15219, CYS16215).

References

[1] J. Lindenmann, V. Matzi, N. Neuboeck, B. Ratzenhofer-Komenda, A. Maier, F.M. Smolle-Juettner, Severe hydrogen sulphide poisoning treated with 4-dimethylaminophenol and hyperbaric oxygen, Div. Hyperb. Med. 40 (2010) 213–217.

[2] C.Y. Su, A.Y. Lu, C.Y. Wu, Y.T. Li, K.K. Liu, W. Zhang, S.Y. Lin, Z.Y. Juang, Y.L. Zhong, F.R. Chen, L.J. Li, Direct formation of wafer scale graphene thin layers on insulating substrates by chemical vapor deposition, Nano Lett. 11 (2011) 3612–3616.

[3] H. Fei, R. Ye, G. Ye, Y. Gong, Z. Peng, X. Fan, E.L.G. Samuel, P.M. Ajayan, J.M. Tour, Boron- and nitrogen-doped graphene quantum dots/graphene hybrid nanoplatelets as efficient electrocatalysts for oxygen reduction, ACS Nano 8 (2014) 10837–10843.

[4] Y.H. Zhang, Y.B. Chen, K.G. Zhou, C.H. Liu, J. Zeng, H.L. Zhang, Y. Peng, Improving gas sensing properties of graphene by introducing dopant and defect: a first-principles study, Nanotech 20 (2009) 185504.

[5] H. Choi, J.S. Choi, J.S. Kim, J.H. Choe, K.H. Chung, J.W. Shin, J.T. Kim, D.H. Youn, K.C. Kim, J.I. Lee, S.Y. Choi, P. Kim, C.G. Choi, Y.J. Yu, Flexible and transparent gas molecule sensor integrated with sensing and heating graphene layers, Small 10 (2014) 3685–3691.

[6] Z. Tan, X. Hao, Y. Shao, Y. Chen, X. Li, P. Fan, Phase modulation and structural effects in a D-shaped all-solid photonic crystal fiber surface plasmon resonance sensor, Opt. Express 22 (2014) 15049–15063.

[7] V.P. Minkovich, D. Monzón-Hernández, J. Villatoro, G. Badenes, Microstructured optical fiber coated with thin films for gas and chemical sensing, Opt. Express 14 (2006) 8413–8418.

[8] J. Mathew, Y. Semenova, G. Farrell, Effect of coating thickness on the sensitivity of a humidity sensor based on an Agarose coated photonic crystal fiber interferometer, Opt. Express 21 (2013) 6313–6320.

[9] T. Han, Y.G. Liu, Z. Wang, J.Q. Guo, Z.F. Wu, S.X. Wang, Z.L. Li, W.Y. Zhou, Unique characteristics of a selective-filling photonic crystal fiber Sagnac interferometer and its application as high sensitivity sensor, Opt. Express 21 (2013) 122–128.

[10] Y. Zhao, G.X. Li, L. Cai, Y. Yang, Refractive index sensing based on photonic crystal fiber interferometer structure with up-tapered joints, Sens. Actuators B: Chem. 221 (2015) 406–410.

[11] F.C. Favero, R. Spittel, F. Just, J. Kobelke, M. Rothhardt, H. Bartelt, A miniature temperature high germanium doped PCF interferometer sensor, Opt. Express 21 (2013) 30266–30274.

[12] D. Wu, Y. Zhao, J. Li, PCF taper-based Mach-Zehnder interferometer for refractive index sensing in a PDMS detection cell, Sens. Actuators B: Chem. 213 (2015) 1–4.

[13] J. Sun, C.C. Chan, Photonic bandgap fiber for refractive index measurement, Sens. Actuators B: Chem. 128 (2007) 46–50.

[14] S.H. Kassani, J. Park, Y. Jung, J. Kobelke, K. Oh, Fast response in-line gas sensor using C-type fiber and Ge-doped ring defect photonic crystal fiber, Opt. Express 21 (2013) 14074–14083.

[15] J. Villatoro, M.P. Kreuzer, R. Jha, V.P. Minkovich, V. Finazzi, G. Badenes, V. Pruneri, Photonic crystal fiber interferometer for chemical vapor detection with high sensitivity, Opt. Express 17 (2009) 1447–1453.

[16] S. Zheng, Y. Zhu, S. Krishnaswamy, Fiber humidity sensors with high sensitivity and selectivity based on interior nanofilm-coated photonic crystal fiber longperiod gratings, Sens. Actuators B: Chem. 176 (2013) 264–274.

[17] J. Sun, C.C. Chan, X.Y. Dong, P. Shum, High-resolution photonic bandgap fiber-based biochemical sensor, J. Biomed. Opt. 12 (2007) 044022.

[18] X. Yu, P. Shum, G.B. Ren, N.Q. Ngo, Photonic crystal fibers with high index infiltrations for refractive index sensing, Opt. Commun. 281 (2008) 4555–4559.

[19] Z. He, F. Tian, Y. Zhu, N. Lavlinskaia, H. Du, Long-period gratings in photonic crystal fiber as an optofluidic label-free biosensor, Biosens. Bioelectron. 26 (2011) 4774–4778.

[20] W. Shin, Y.L. Lee, B.A. Yu, Y.C. Noh, T.J. Ahn, Highly sensitive strain and bending sensor based on inline fiber Mach–Zehnder interferometer in solid core large mode area photonic crystal fiber, Opt. Commun. 283 (2010) 2097–2101.

[21] Y. Zhu, Z. He, J. Kaňka, H. Du, Numerical analysis of refractive index sensitivity of long-period gratings in photonic crystal fiber, Sens. Actuators B: Chem. 129 (2008) 99–105.

[22] L. Rindorf, O. Bang, Highly sensitive refractometer with a photonic crystal fiber long-period grating, Opt. Express 33 (2008) 563–565.

[23] L. Rindorf, J.B. Jensen, M. Dufva, L.H. Pedersen, O. Bang, Photonic crystal fiber long-period gratings for biochemical sensing, Opt. Express 14 (2006) 8224–8231.

[24] L. Rindorf, O. Bang, Sensitivity of photonic crystal fiber grating sensors: biosensing, refractive index, strain, and temperature sensing, J. Opt. Soc. Am. B 25 (2008) 310–324.

[25] Y.J. Rao, D.W. Duan, Y.E. Fan, T. Ke, M. Xu, High-temperature annealing behaviors of CO_2 laser pulse-induced long-period fiber grating in a photonic crystal fiber, J. Lightwave Technol. 28 (2010) 1530–1535.

[26] Q. Shi, B.T. Kuhlmey, Optimization of photonic bandgap fiber long period grating refractive-index sensors, Opt. Commun. 282 (2009) 4723–4728.

[27] C. Tao, H. Wei, W. Feng, Photonic crystal fiber in-line Mach-Zehnder interferometer for explosive detection, Opt. Express 24 (2016) 2806–2817.

[28] C. Tao, H. Wei, Y. Zhu, S. Krishnaswamy, Grapefruit photonic crystal fiber sensor for gas sensing application, Opt. Eng. 55 (1) (2016) (057103. 1-057103.8).

[29] J. Villatoro, V. Finazzi, G. Badenes, V. Pruneri, Highly sensitive sensors based on photonic crystal fiber modal interferometers, J. Sens. 2009 (2009) 747803.

[30] B.H. Lee, J. Nishii, Dependence of fringe spacing on the grating separation in a long-period fiber grating pair, Appl. Opt. 38 (1999) 3450–3459.

[31] L. Niu, C.L. Zhao, H. Gong, Y. Li, S. Jin, Curvature sensor based on two cascading abrupt-tapers modal in terferometer in single model fiber, Opt. Commun. 333 (2014) 11–15.

[32] J. Villatoro, V. Finazzi, V.P. Minkovich, V. Pruneri, G. Badenes, Temperature-insensitive photonic crystal fiber interferometer for absolute strain sensing, Appl. Phys. Lett. 91 (2007) 091109.

[33] C.L. Zhao, X. Yang, C. Lu, W. Jin, M.S. Demokan, Temperature-insensitive interferometer using a highly birefringent photonic crystal fiber loop mirror, IEEE Photonics Tech. Lett. 16 (2004) 2535–2537.

[34] O. Frazao, J.M. Baptista, J.L. Santos, Temperature-independent strain sensor based on a Hi-Bi photonic crystal fiber loop mirror, IEEE Sens. J. 7 (2007) 1453–1455.

Biographies

Xu Feng obtained his BS degree in electronics and information engineering from Chongqing Three Gorges University, China in 2014. He is studying for his MS degree in Chongqing University of Technology. Now, his research interests include the gas sensing application of the photonic crystal fiber.

Wenlin Feng is currently a professor of School of Science in Chongqing University of Technology, Chongqing, China. He got his Ph.D. degree from Sichuan University, Chengdu, China in 2008. He was Optical Engineering Post-doctoral Fellow at Chongqing University, Chongqing, China from 2009 to 2011. He was also associated as a Visiting Scientist at Tsinghua University, Beijing, China in 2011, University of Arkansas at Little Rock, USA during 2014–2015. His research interest has been synthesis, modification and application of nanomaterials such as graphene, sensitive membrane, semiconductor, optical fiber sensor, etc., and their functional composites for applications ranging from sensors, energy storage, luminescence, etc. He has published more than 100 research articles in reputed international journals and holds 3 Chinese patents.

Chuanyi Tao received his Ph.D. in Optical Engineering from Chongqing University in 2011. He has been an associate professor of Physics and Energy at Chongqing University of Technology. His research interests are development of fiber-optic sensors for safety monitoring.

Dashen Deng received his BS degree in Communication Engineering from Tianjin University of Technology, China in 2011. Now, he is studying for his MS degree in Chongqing University of Technology, majoring in the optical systems and gas-sensing application of functional materials.

Xiang Qin received his BS degree in Electronic Information Science and Engineering from Datong University, China in 2011. Now, he is studying for his MS degree in Chongqing University of Technology, majoring in optical material and optical fiber gas sensor.

Rong Chen received her BS degree in Communication Engineering from Neijiang Normal University, China in 2012. Now, she is studying for her MS degree in Chongqing University of Technology, majoring in photoelectric information acquisition and processing.